RAPID COMMUNICATIONS

PHYSICAL REVIEW A VOLUME 44, NUMBER 12 15 DECEMBER 1991

Wetting in a confined geometry: A Monte Carlo study

Andrea J. Liu* and Gary S. Grest

Corporate Research Science Laboratory, Exxon Research and Engineering Company, Annandale, New Jersey 08876

(Received 12 July 1991)

Binary liquid mixtures are expected to display two interfacial transitions when confined in small pores. One is a wetting transition, similar to such transitions on planar substrates. The other is an interfacial shape transition. We use Monte Carlo simulations to show that an Ising system displays both transitions. We find a wetting phase diagram similar to that of a model with a long-ranged wetting potential, proving that the existence of both transitions is insensitive to the wetting potential shape.

PACS number(s): 68.45.Gd, 64.60.−i, 47.55.Mh

Binary liquid mixtures display radically altered phase behavior when imbibed into porous media. In bulk, binary liquids separate into two phases below the critical mixing point. By contrast, in porous glasses the two phases form many small domains, even far below the critical point [1–3]. It is well accepted that preferential attraction of one phase to the pore surface plays a major role in preventing macroscopic phase separation. It is also clear that the geometry of the porous medium must affect the phase behavior. Whether the observed small-domain structure is due to the *randomness* of the pore structure or to the *confinement* of the liquids in small pores is, however, controversial. One possibility is that randomness of the pore structure causes random-field Ising-like behavior, which leads to small domains [4]. An alternate suggestion is that confinement in small pores slows down domain growth in certain regions of the wetting phase diagram; thus, macroscopic phase separation is not observed because the kinetics are too slow [5]. Liu *et al.* [5] argue that the kinetics are strongly influenced by the wetting behavior. Therefore, knowledge of the wetting phase diagram is essential for understanding domain growth in confined geometries.

In this paper, we use Monte Carlo (MC) simulations to study the wetting phase diagram of an Ising model confined in a pore. Such simulations have proven invaluable in the study of wetting on *planar* surfaces [6,7], because theoretical studies of wetting phase diagrams have mainly been limited either to mean-field theory [8–10] or to phenomenological treatments based on the effective interface potential approximation [11,12]. In the case of wetting in a cylindrical pore, the phenomenological theory described in Ref. [5] required assumptions beyond those normally employed for a planar substrate. Finite-size shifts of the critical point were ignored and assumptions were made about the structure of the complete and partial wetting configurations. The MC results test the sensitivity of the wetting phase diagram to the shape of the effective interface potential, because the wetting forces are short ranged for the Ising model and long ranged in the phenomenological theory.

The results of Ref. [5] are summarized by the phase diagram in Fig. 1 for a cylindrical pore of diameter $L_\perp$ and length $L_z \gg L_\perp$ filled with a binary liquid mixture of fixed critical composition. There are three distinct phases. The partial-wetting "plug" consists of a region of phase α separated from a region of phase β by the $\alpha\beta$ interface stretching across the pore. The complete wetting "capsule" consists of a single long bubble of the nonwetting phase β suspended in the center of the pore and surrounded by the wetting phase α. The "tube" is a capsule of minimum radius, corresponding to $r = L_\perp/2\sqrt{2}$ when the β phase occupies half of the volume.

Our aim is to test the results in Fig. 1 using MC techniques. We exploit the standard mapping of a binary liquid mixture onto a lattice-gas model, where A and B molecules correspond to $S_i = \pm 1$, respectively; S_i denotes the orientation of the spin at site i in the lattice. The wetting forces are purely short ranged; we assume that a field H_1 acts on the first layer only, and interactions between spins are limited to nearest neighbors. We study an $L_\perp \times L_\perp \times L_z$, parallelopiped. Our system sizes are $L_\perp = 14, 20, 28$ and L_z ranging from $L_z = 40$ to 320. (For $L_\perp < 14$, the wetting layer should be less than two layers thick for equal composition of A and B [5]. Since the wetting transition is difficult to locate if the wetting layer is too thin, we choose $L_\perp \geq 14$.) Periodic boundary conditions are imposed in the long (L_z) direction, and surface fields and couplings are imposed along the four surfaces.

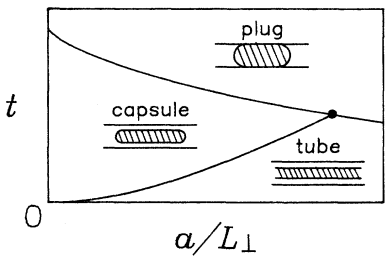

FIG. 1. Phenomenological wetting phase diagram for a binary liquid mixture confined in a cylindrical pore of diameter $L_\perp$, showing the three configurations of tubes, capsules, and plugs (with the nonwetting phase hatched in) and their corresponding transition lines (solid). The reduced temperature $t \equiv (T_c^0 - T)/T_c^0$ is positive in the two-phase region, and a is a molecular length. The model assumes a van der Waals effective interface potential.

The Hamiltonian is

$$\mathcal{H} = -J \sum_{\text{bulk}} S_i S_j - J_1 \sum_{\text{surfaces}} S_i S_j - H_1 \sum_{\text{surfaces}} S_i \ , \quad (1)$$

where $S_i = \pm 1$, J is the coupling between bulk spins, J_1 is the coupling between surface spins, and $H_1 > 0$ is the surface field. The three-dimensional Ising model on a simple cubic lattice has a critical point at $J/k_B T_c^0 \approx 0.221\,63$[13]. In these simulations, the temperature T always satisfies $T < T_c^0$.

In order to study wetting, we fix the magnetization inside the pore [5,14] by using Kawasaki spin-exchange dynamics. In all runs, we choose equal numbers of up and down spins so that the total magnetization is zero. To avoid long diffusion times associated with exchanging spins on nearest neighbors, we allow spin exchange between pairs of spins located arbitrarily far apart. This enables the system to equilibrate more quickly.

Most of the analysis is based on the magnetization profile, obtained as follows. For each square cross section along the pore length, we average over square rings. The four spins in the innermost ring are averaged to obtain $m(r=1,z)$ for each z. Similarly, the $4(2n-1)$ spins in the nth ring are averaged to obtain $m(r=n,z)$, etc. The resulting $m(r,z)$ is then averaged over 50 Monte Carlo exchanges per spin (MCS). Contour plots of magnetization profiles are shown for several temperatures in Fig. 2. The profiles were reflected around the center axis. $m=+1$ is red while $m=-1$ is violet; intermediate values are given by the spectrum. At low T, we obtain the partial wetting plug, shown in Fig. 2(a). The difference between the α (red) and β (violet) phases is pronounced and the $\alpha\beta$ interface is sharp. At higher T, the system undergoes a wetting transition and we obtain the capsule, shown in Figs. 2(b) and 2(c). The capsule shape is approximately a cylinder with spherical endcaps, as assumed in Ref. [5]. At still higher T we obtain the tube, shown in Fig. 2(d). Thus, the assumption of plug, capsule, and tube configurations in Ref. [5] is well justified; the contour plots clearly confirm their existence.

The widths of the interfaces shown in Figs. 2(b)–2(d) appear thicker than the correlation length, which is about one lattice spacing. This is due to capillary wave fluctuations which are averaged over 50 MCS.

We turn now to transitions between the plug, capsule, and tube configurations. The initial configuration was always a plug with the $\alpha\beta$ interface running across the pore (initial contact angle of 90°). To locate the transitions, we first made a temperature sweep, raising T by $k_B \Delta T = 0.1J$ and running for 10 000 MCS at each T to approximately locate the transitions. We found no change in the variance or mean of the energy after roughly the first 7500 steps. The transitions were then determined more carefully by using the configuration saved at T just below the transition region, and warming in smaller jumps. After increasing T, we sometimes waited for up to 25 000 MCS to make sure the system had reached equilibrium.

The plug-capsule or *wetting* transition is determined as follows. Since the surface field H_1 is positive, the nonwetting phase β has $m < 0$. Below the wetting transi-

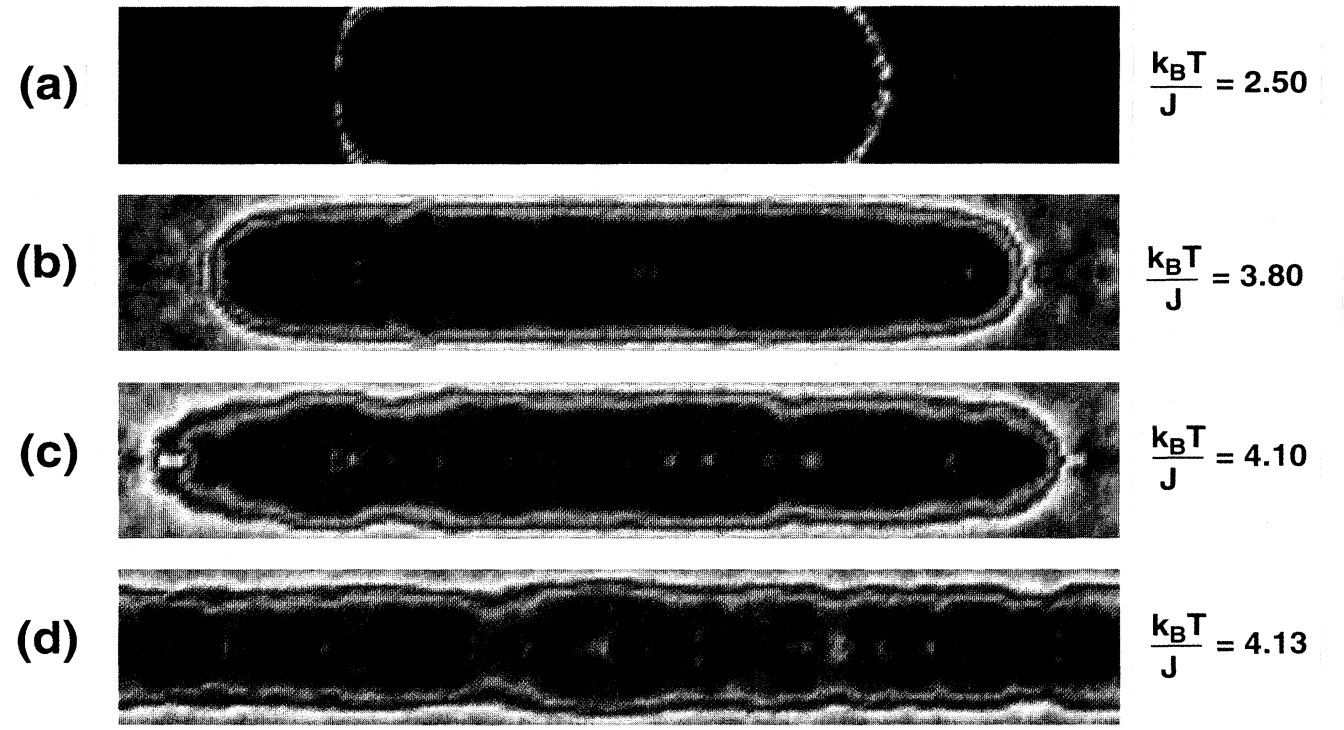

FIG. 2. Magnetization profiles showing the (a) plug, (b) and (c) capsule, and (d) tube configurations for a $28 \times 28 \times 160$ system. Magnetization $m = +1$ is red and $m = -1$ is violet; intermediate values are given by the spectrum.

tion, the β phase touches the wall, so the magnetization of the outermost shell $m(L_\perp/2,z)$ is negative for some values of z. We defined the wetting transition T_w as the lowest T above which the magnetization of the outermost shell satisfies $m(L_\perp/2,z)>0$ for *all* z. By contrast, Binder and Landau [7] used the surface excess magnetization and energy to locate the wetting transition on planar substrates. Thermodynamic criteria fail in our case because of the constraint of fixed magnetization. We found the transition was sufficiently broad that our criterion sufficed. Different criteria, such as the T dependence of the average surface magnetization, or the condition $m(L_\perp/2,z)>m^+_{\rm bulk}$, yield different estimates which lie within the error bars; the qualitative trends we present should be reliable.

The transition from capsule to tube is an interfacial shape transition, as shown in Figs. 2(b)–2(d). The capsule in Fig. 2(b) is at T well below the capsule-tube boundary. At higher T, the capsule grows longer and thinner, as shown in Fig. 2(c) and predicted in Liu *et al.* [5]. As T is raised further, the capsule grows long enough for the two ends to meet and becomes the tube shown in Fig. 2(d). Thus, the capsule-tube boundary, or *interfacial shape transition* $T_{\rm ct}$, is defined as the lowest T above which the magnetization of the *innermost* shell satisfies $m(1,z)<0$ for *all* z. The transition is very sharp.

The wetting phase diagram is shown as a function of $L_\perp$ in Fig. 3(a). We studied the wetting transition and capsule-tube boundary for $L_\perp=14,20,28$ for $H_1/J=0.7$ and $J_1/J=1$. Figure 3(a) shows that the wetting transition moves closer to the critical point as the pore size decreases. This behavior is qualitatively similar to phenomenological results as shown in Fig. 1. Note that in our simulation, the wetting forces are short-ranged contact forces, the wetting transition for these parameter values is second order (see discussion below), and the pore has a square cross section. By contrast, in the theory of Ref. [5], the wetting forces are long-ranged van der Waals forces, the wetting transition is first order, and the pore has a circular cross section. The similarity between Figs. 1 and 3(a) demonstrates that the results of Ref. [5] are remarkably robust: the topology of the phase diagram is not affected by the specific nature of the interface wetting potential, the order of the wetting transition, or the shape of the pore cross section.

The surface field H_1/J was varied for $L_\perp=14$ and $J_1/J=1$ to locate the phase boundaries shown in Fig. 3(b). As expected, the wetting transition moves closer to the critical point as the surface field decreases. The tube disappears entirely for $H_1/J\gtrsim 0.3$. In contrast, the tube exists for any nonzero value of the surface field when the wetting potential is van der Waals [5]. We believe that the difference lies in the range of interactions; when the range is finite, the tube phase can disappear at a nonzero value of H_1/J. Experimentally, H_1 can be varied by altering the pore surface chemistry [15].

Finally, we varied J_1/J at fixed $H_1/J=0.3$, 0.5, and 0.7. As J_1/J increases, T_w and T_{ct} move further away from the critical point and the capsule region shrinks. At $H_1/J=0.5$ and $J_1/J\approx 1.2$, the capsule disappears; there is a direct transition from plug to tube. This is similar to the "triple point" predicted in Ref. [5] as shown in Fig. 1.

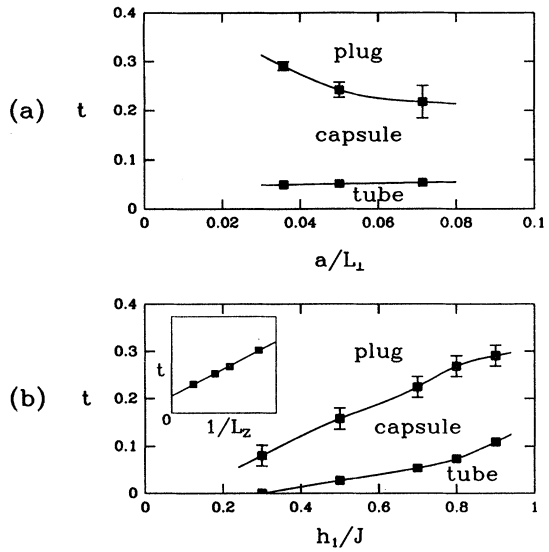

FIG. 3. Phase diagrams for (a) reduced temperature $t\equiv(T_c^0-T)/T_c^0$ vs $a/L_\perp$ where a is the lattice spacing and $L_\perp$ is the pore diameter, and (b) t vs H_1/J. Plot (a) should be compared to Fig. 1. $J_1/J=1$ in both plots, $H_1/J=0.7$ in (a), and $L_\perp=14$ in (b). Lines are to guide the eye. The inset in (b) shows finite-size shifts in the interfacial shape transition $T_{ct}(L_z)$; the line is a least-squares fit.

The phase diagrams shown in Fig. 3 show the transition temperatures in the limit $L_z\to\infty$. T_w is not sensitive to L_z within the error bars. The error bars are large because of finite-size rounding of the transition, and shrink rapidly as the pore diameter $L_\perp$ increases. The interfacial shape transition, on the other hand, depends strongly on L_z. The inset of Fig. 3(b) is a finite-size scaling plot of the reduced transition temperature $t\equiv[T_c^0-T_{ct}(L_z)]/T_c^0$ as a function of $1/L_z$ for $L_\perp=14$. The linear relationship can be understood by assuming that the capsule endcaps contribute a constant term to the free energy, or a $1/L_z$ term to the free energy per unit length. If we expand the transition temperature around $T_{ct}(L_z\to\infty)$, then $T_{ct}(L_z)-T_{ct}(\infty)$ is proportional to the difference in free energy per unit length, which is proportional to $1/L_z$.

The order of the transitions was studied by performing warming and cooling runs. All of the runs previously described were warming runs, starting with a plug and raising T in steps, then running for 10 000 MCS t each T. We also performed cooling runs, starting with a tube and lowering T in a similar fashion. The tube remains metastable far below T_{ct}. This is demonstrated in Fig. 4, where we plot energy U/J per spin versus T. The energy is averaged over the last 2500 out of the 10 000 MCS run at each T. The energies from warming and cooling runs are plotted as open and solid squares, respectively. The warming and cooling runs coincide above T_{ct}, where the tube is stable. Below T_{ct}, however, where the capsule

phase is stable, the results differ [16]. In order to transform from the tube to a capsule, the tube must pinch off—the wetting phase must nucleate in the center of the pore. When the tube pinches off to form a capsule, the energy drops to the lower branch. The hysteresis at T_{ct} implies that the interfacial shape transition is *first order.* By contrast, there is no observable hysteresis at T_w (marked by an arrow in Fig. 4), indicating that the wetting transition is *second order* for these values of H_1, J_1, and $L_\perp$.

We believe that the wetting transition is second order for *all* parameters values in Fig. 3. According to the wetting phase diagrams obtained by Nakanishi and Fisher [9] for planar substrates, there should be a wetting tricritical point for some H_1^t when $J_1/J \lesssim 1.5$. For $H_1 < H_1^t$ the wetting transition is second order and for $H_1 > H_1^t$ the transition is first order. Moreover, Nakanishi and Fisher predicted that H_1^t decreases as J_1 increases. This was verified by Binder and Landau [7] for the planar case (see their Fig. 10). Our results for the confined geometry are similar; this was established by studying the average surface magnetization as a function of H_1/J for fixed J_1/J at several T. We find that the transitions are first order for $J_1/J=1.2$ and $H_1/J \gtrsim 0.7$. For $J_1/J=1.0$, the wetting transition is second order for $H_1/J < 1.0$; we have not studied larger values of H_1. These results show that the wetting transition lines are second order in Fig. 3. They also show that H_1^t exists and decreases as J_1 increases, as predicted in the planar case.

In summary, the simulations show that wetting phase diagrams are richer for confined geometries than for a planar surface. There are, however, many qualitative similarities between wetting in a pore and on a plane, such as the wetting tricritical point. This agrees well with recent work of Swift *et al.* [14], which shows that similar wetting transitions occur between two plates, and that the transitions approach the usual planar transitions as the plate spacing diverges. Thus, the wetting phase diagrams for confined geometries should be describable by adding another axis, corresponding to $1/L_\perp$, to the phase diagrams of Nakanishi and Fisher [9].

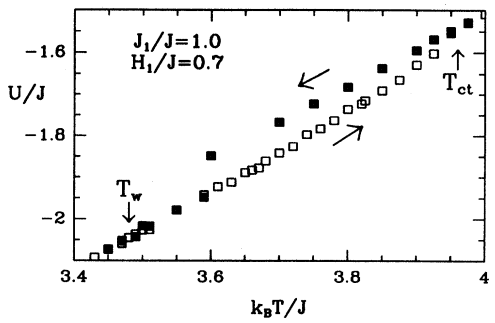

FIG. 4. Plot of average energy U/J vs $k_B T/J$ for warming runs (open squares) and cooling runs (solid squares) on a $20\times20\times80$ system. The wetting transition T_w and interfacial shape transition T_{ct} are marked by arrows. There is hysteresis at the first-order interfacial shape transition, but not at the second-order wetting transition.

In addition, this work verifies the assumptions underlying Ref. [5]. The plug, capsule, and tube configurations clearly exist, and the wetting phase diagram is qualitatively consistent with the predicted one in Fig. 1. Although the interface wetting potential was assumed to be long ranged in Ref. [5] and is short ranged in this simulation, the qualitative picture is the same. Finite-size shifts of the critical temperature do not appear to substantially alter the picture, either. Thus, the phenomenological theory is quite insensitive to the details of the model.

We appreciate useful discussions with W. Klein, M. W. Fisher, and L. Monette.

*Present address: Materials Department, University of California, Santa Barbara, CA 93106.

[1] S. B. Dierker and P. Wiltzius, Phys. Rev. Lett. **58**, 1865 (1987); **66**, 1185 (1991).

[2] M. C. Goh, W. I. Goldburg, and C. M. Knobler, Phys. Rev. Lett. **58**, 1008 (1987).

[3] M. Y. Lin and S. K. Sinha (unpublished).

[4] F. Brochard and P. G. de Gennes, J. Phys. Lett. (Paris) **44**, 785 (1983); P. G. de Gennes, J. Phys. Chem. **88**, 6469 (1984).

[5] A. J. Liu, D. J. Durian, E. Herbolzheimer, and S. A. Safran, Phys. Rev. Lett. **65**, 1897 (1990).

[6] K. Binder, D. P. Landau, and D. M. Kroll, Phys. Rev. Lett. **56**, 2272 (1986).

[7] K. Binder and D. P. Landau, Phys. Rev. B **37**, 1745 (1988).

[8] D. E. Sullivan and M. M. Telo da Gama, in *Fluid Interfacial Phenomena,* edited by C. A. Croxton (Wiley, New York, 1986), p. 45.

[9] H. Nakanishi and M. E. Fisher, Phys. Rev. Lett. **49**, 1565 (1982).

[10] C. Ebner, W. F. Saam, and A. K. Sen, Phys. Rev. B **32**, 1558 (1985); C. Ebner and W. F. Saam, Phys. Rev. Lett. **58**, 587 (1987).

[11] P. G. de Gennes, C. R. Acad. Sci. (Paris) Ser. II **297**, 9 (1983).

[12] R. Lipowsky, Z. Phys. B **55**, 345 (1984).

[13] A. J. Liu and M. E. Fisher, Physica A **156**, 35 (1989).

[14] M. R. Swift, A. L. Owczarek, and J. O. Indekeu, Europhys. Lett. **14**, 475 (1991).

[15] D. J. Durian and C. Franck, Phys. Rev. Lett. **59**, 555 (1987); **59**, 1492 (1987).

[16] The transition should be located by where the *free* energies, rather than energies, of the capsule and tube cross. However, the difference in entropy arises mostly from the possible positions of the entire capsule along the pore, and should be small for any physically attainable pore-aspect ratio. (The configurational entropy is, of course, important when the pore-aspect ratio $L_z/L_\perp$ diverges, since there is no long-range order in one dimension.) By neglecting entropy, we slightly overestimated the free energy of the capsule. Thus, the transition must occur at the upper end of the hysteresis region.

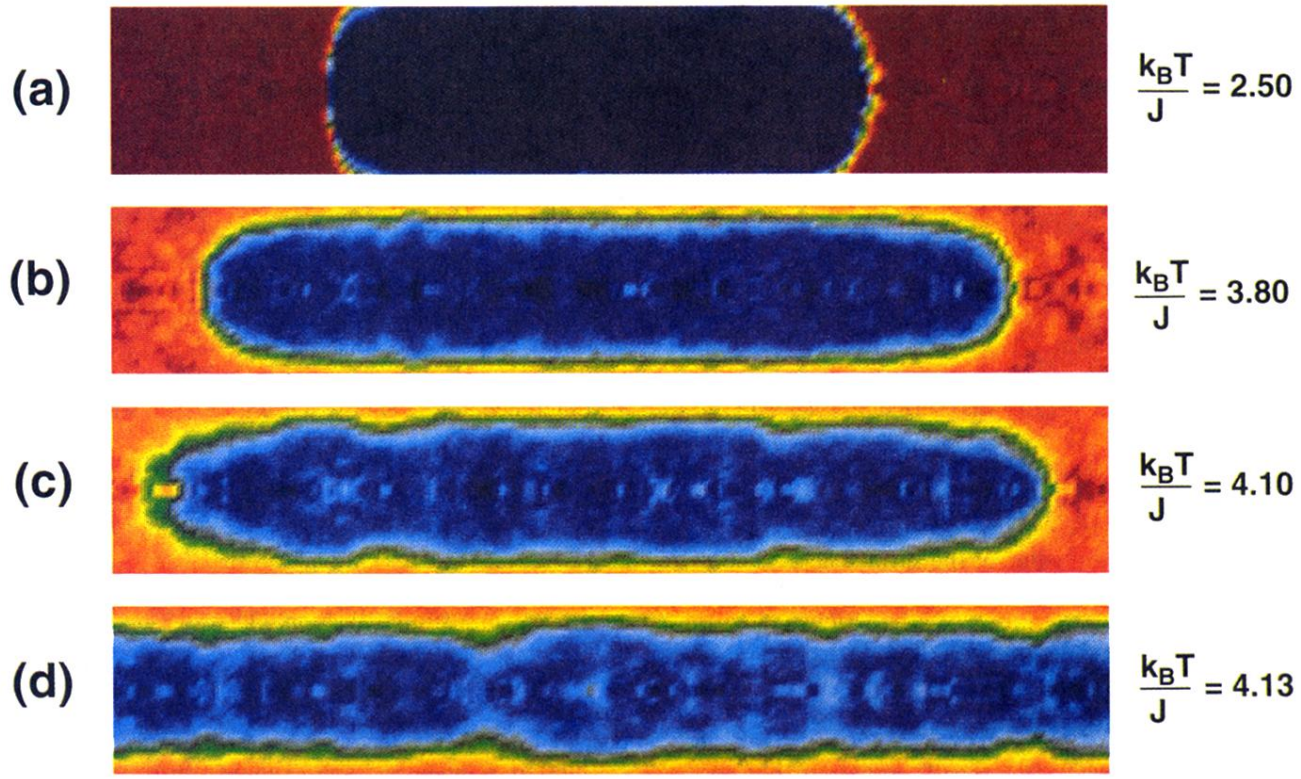

FIG. 2. Magnetization profiles showing the (a) plug, (b) and (c) capsule, and (d) tube configurations for a $28 \times 28 \times 160$ system. Magnetization $m = +1$ is red and $m = -1$ is violet; intermediate values are given by the spectrum.